NASA/TP-1998-208707

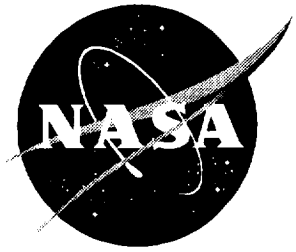

Track Structure Model for Radial Distributions of Electron Spectra and Event Spectra From High-Energy Ions

F. A. Cucinotta
Langley Research Center, Hampton, Virginia

R. Katz
University of Nebraska, Lincoln, Nebraska

J. W. Wilson
Langley Research Center, Hampton, Virginia

National Aeronautics and
Space Administration

Langley Research Center
Hampton, Virginia 23681-2199

September 1998

Available from the following:

NASA Center for AeroSpace Information (CASI)
7121 Standard Drive
Hanover, MD 21076-1320
(301) 621-0390

National Technical Information Service (NTIS)
5285 Port Royal Road
Springfield, VA 22161-2171
(703) 487-4650

Abstract

An analytic method is described for evaluating the average radial electron spectrum and the radial and total frequency-event spectrum for high-energy ions. For high-energy ions, indirect events make important contributions to frequency-event spectra. The method used for evaluating indirect events is to fold the radial electron spectrum with measured frequency-event spectrum for photons or electrons. The contribution from direct events is treated using a spatially restricted linear energy transfer (LET). We find that high-energy heavy ions have a significantly reduced frequency-averaged lineal energy (y_F) compared to LET, while relativistic protons have a significantly increased y_F and dose-averaged lineal energy (y_D) for typical site sizes used in tissue equivalent proportional counters. Such differences represent important factors in evaluating event spectra with laboratory beams, in spaceflight, or in atmospheric radiation studies and in validation of radiation transport codes. The inadequacy of LET as descriptor because of deviations in values of physical quantities, such as track width, secondary electron spectrum, and y_D for ions of identical LET is also discussed.

Introduction

This paper presents an analytic model for describing the radial distribution of electrons and frequency-event spectra measured by proportional counters used in the dosimetry of radiation fields in space and the upper atmosphere (refs. 1 and 2). At high energies the track width of an ion will extend to 100's of microns or more because of delta-ray diffusion. Monte-Carlo models have difficulty with these calculations because of large computational times and poor statistics in considering events at distances greater than 1 μm from the track of an ion (ref. 3). Furthermore, in most applications with high-energy nuclei including space or atmospheric radiation studies, nuclear fragmentation and energy loss processes will lead to a broad spectrum of ion types and velocities. These considerations point to the usefulness of analytic approaches to treat track structure for high-energy particles. An analytic model is developed to evaluate frequency-event spectra that include the indirect events important for high-energy ions. Furthermore, the radial dependence of the spectrum is described. The model is being used to compare the results of radiation transport codes directly to recent spaceflight measurements as described elsewhere. These comparisons will provide important validation of radiation transport codes and environmental models.

Track structure models describe the relationship between the spatial distribution of energy deposition in the form of positions of ionization and excitation, the geometric structure of target molecules, and the response of a physical or biological system. The first track model formulated was the average-track model, or amorphous-track model, which considered the radial dose about the path of the ion as the descriptive parameter for ion effects. This model has been used for over 30 years in describing the response of physical and biological systems (refs. 4–6). The average-track model has the advantage of simplicity; however, the model considers only simplified target geometry and ignores fluctuations in energy deposition. Monte-Carlo track simulations consider local fluctuations in energy deposition and provide methods for dealing with complicated target geometry including applications to treat details of DNA molecular structure and DNA folding (refs. 7 and 8). However, the average-track model remains the most successful parametric approach for describing the response of biological systems and physical detectors to ions.

The importance of track width has been discussed for many years in relationship to radiation quality and the resulting inadequate capability of linear energy transfer (LET) or the ratio of the square of the effective charge to ion velocity (Z^{*2}/β^2) as indicators of biological effectiveness (ref. 9). The parameter Z^{*2}/β^2 was noted by Katz to be useful only when comparing ions of similar velocity (ref. 9). Experimental observation of the importance of track width has been demonstrated for endpoints such as inactivation of yeast, bacterial and V79 mammalian cells, and mutation of the HPRT gene in V79 cells (refs. 10–12). Recently,

calculations with the average-track model (ref. 6) showed that, for cellular mutation, the spatial distribution of sites for cellular inactivation and gene mutation necessitates the use of a track structure description for radiation quality that indicates the inadequacy of the parameters LET or Z^{*2}/β^2. Our calculation of the radial distribution further illustrates inadequacies in these parameters when biological effectiveness is dependent on electron energy.

Algorithms for converting particle energy spectra to lineal energy spectra are needed to correlate radiation transport code predictions to lineal energy spectra measured by proportional counters. Microdosimetric approaches to energy deposition have relied mostly on Monte-Carlo simulations (refs. 13 and 14), which are computationally inadequate for describing diverse radiation fields such as that seen in space or in the upper atmosphere. Several factors are known to be important in evaluating lineal energy spectra. For high-energy ions, a significant fraction of events occur from secondary electrons produced by ions that do not directly enter the volume of the detector. Other factors include the treatment of secondary electrons transported outside the volume by ions that do pass through the volume, nuclear reaction effects, and the effects of straggling of the ions in the volume. For each of these factors the role of wall composition and thickness must be studied. Also, for low-energy ions there is a significant change in the rate of energy loss inside the volume, including the effects of stopping ions (ref. 15).

This report presents an approach for treating the indirect events from delta rays and introduces a spatially restricted energy deposition model for direct events. The other factors noted will be discussed elsewhere.

Model for Radial Electron Spectrum

The approach of the average-track model has been to consider the primary electron spectrum from ion interactions with target atoms and fold this spectrum with average transmission properties of electrons to obtain the spatial distribution of electron dose as a function of radial distance from the path of the ion. As introduced by Kobetich and Katz (ref. 4) the radial dose is given by

$$D_\delta(t) = \frac{-1}{2\pi t} \sum \int d\Omega \int d\omega \frac{\partial}{\partial t} [E(t, \omega)\eta(t, \omega)] \times \eta(t, \omega)\left(\frac{dn_i}{d\omega}\, d\Omega\right) \quad (1)$$

In equation (1) E is the residual energy of an electron ω after travelling distance t, and $\eta(t,\omega)$ is the transmission probability that an electron with starting energy ω penetrates a depth t. We have included an angular distribution for the primary electrons with energy ω and solid angle Ω. The subscript δ indicates that it is the dose contribution from ionization by secondary electrons at a radial distance t from the path of the ion. The input functions for the evaluation of equation (1) are described by Cucinotta et al. (ref. 16). Note that the cross sections for electron production from protons are scaled to heavy ions using effective charge.

The LET can be described by integrating the radial dose distribution over all radial distances and including other contributions such as excitations, nuclear stopping, and high-energy corrections (ref. 17)

$$\text{LET} = 2\pi \int^{t_M} t\, dt[D_\delta(t) + D_{\text{exc}}(t)] + \text{Nuclear stopping} + \text{High-energy corrections} \quad (2)$$

where t_M is the maximum distance of electron penetration. Brandt and Ritchie (ref. 18) have considered a formulation of the excitation term, $D_{\text{exc}}(t)$, as

$$D_{\text{exc}}(t) = C_{\text{exc}} \exp(-t/2d)/t^2 \quad (3)$$

with $d = \beta/2\ \omega_r$ with $\omega_r = 13$ eV for water. The radially restricted LET can be introduced by limiting the upper limit in equation (2) as defined by

$$L_r = 2\pi \int^{r} t\, dt[D_\delta(t) + D_{\text{exc}}(t)] \quad (4)$$

Equation (4) ignores the nuclear stopping and high-energy corrections to the LET. In many applications the number of electrons, as well as their energy spectrum, is required for describing the response of a system. The average or residual energy spectrum of electrons penetrating to a radial distance t is derived from equation (1) as

$$\phi(t, E) = \frac{1}{2\pi t} \sum \int d\Omega \frac{S(\omega)}{S(E)} \times \left\{ \eta(t, E) + \left[\frac{E}{S(E)} \right] \frac{\partial \eta(t, E)}{\partial t} \right\} \left(\frac{dn_i}{d\omega} d\Omega \right) \quad (5)$$

where the primary electron energy ω is now a function of the residual energy. Equation (5) shows that the attenuation of the electron spectrum is through two factors: first an overall factor of $1/t$ for all secondary electrons, and second an additional attenuation for low-energy electrons dependent on their starting energy and depth of penetration.

Figures 1 and 2 show calculations of the radial dose for ions of linear energy transfer (LET) of 30 and 150 keV/μm. These results show the large differences in radial energy deposited due to differences in track width, which is dependent on ion velocity. Such differences are expected to be important for specific target molecule sizes and the spatial distribution of these molecules. Also shown in figure 1 are results based on an assumption that the electrons are ejected normal to the ion path leading to an underestimate of the dose at small distances. Figures 3 and 4 show the secondary electron spectrum for these same ions. We have plotted the spectrum from equation (5) versus energy for several impact parameters and also we plot $2\pi tE\ \phi(E, t)$ versus energy on a linear-log scale to show the fractional contribution from each decade of electron energy. Lower charge ions are seen to have both a confined track width and electrons of lower energy (i.e., electrons of higher LET). Experiments with soft X rays indicate increased biological effectiveness for electrons with energies less than several keV (ref. 19).

For ions of a given value of LET, low charge and energy ions (LZE) may have increased effectiveness because the predominance of low-energy electrons in comparison to high charge and energy ions (HZE). However, for large target volumes, including a response dependent on alterations in spatially distributed target molecules, the present energy deposition model would predict that the effects of track width would increase the effectiveness of HZE ions in comparison to LZE ions. The secondary electron spectrum varies more slowly as a function of radial distance for the LZE ions and contains a larger fraction of low-energy electrons both at small radial distances and at the maximal radial distances where the highest energy ejected electrons are stopped (electron track ends). Figures 3 and 4 show that for ions with atomic numbers less than iron ($Z < 26$), overlapping electron tracks in small volumes such as the nucleosome would occur only at very close distances to the path of the ion (<10 nm).

Direct Events

For fast charged ions undergoing small velocity changes in the site, the energy deposited for path length x is given in terms of the linear energy transfer as

$$\varepsilon = Lx \quad (6)$$

For high-energy ions a significant fraction of the LET escapes the volume of a site by electron transport and therefore does not contribute to the events inside the site. The energy deposited, as restricted by the spatial distribution of secondary electrons, is given by

$$\varepsilon = \int dx' L_r(x') \quad (7)$$

For a given path length the radial distance from the ion to the center of the volume is

$$t_x^2 = \frac{d^2 - x^2}{4} \quad (8)$$

where d is the diameter of the site. For a spherical site the relation given by equation (8) limits the radial extension of the track for direct events such that the maximum radial extension of the track at a polar angle φ is given by

$$t_M(x', \varphi) = \sqrt{r_{x'}^2 + t_x^2 - 2 r_{x'}\, t_x \cos \varphi} \quad (9)$$

where

$$r_{x'} = x' \qquad \text{for } x' < d/2 \quad (10a)$$

$$r_{x'} = d - x' \quad \text{for } x' > d/2 \quad (10b)$$

The energy deposited for a given path length as restricted by electron diffusion is then given by

$$\varepsilon = \int^x dx' \int d\varphi \int^{t_M(x', \varphi)} t\, dt\, D(t) \quad (11)$$

For a distribution of path lengths $f(x)$, the distribution of event sizes is given by

$$f(\varepsilon)\, d\varepsilon = Nf(x)\, dx \tag{12}$$

Such that

$$f(\varepsilon) = Nf[\varepsilon(x)]\left(\frac{d\varepsilon}{dx}\right)^{-1} \tag{13}$$

where from equation (11)

$$\frac{d\varepsilon}{dx} = \int d\varphi \int^{t_M(x,\varphi)} t\, dt\, D(t) \tag{14}$$

The lineal energy is given by $y = \varepsilon / x_A$ where x_A is the average path length in the volume and the distribution in lineal energy is given by

$$f(y) = Nx_A f[y(x)]\left(\frac{d\varepsilon}{dx}\right)^{-1} \tag{15}$$

Low velocity ions with insufficient range to transverse the site at a given path length will deposit all their energy in the site and the direct events should be appropriately corrected (ref. 15). The distributions for direct events should also be corrected for ion straggling and nuclear reaction effects should be described.

Indirect Events

Particles that do not pass directly through the volume deposit energy through secondary electrons; these events are denoted as indirect events. Figure 5 shows the fraction of the LET from iron ions as a function of their energy that are from indirect events in a homogeneous medium for several site sizes. At high energies, a significant fraction of the LET from indirect events occurs for site sizes in the 0.5–4 μm range, which is used frequently for radiation field definition. For small site sizes expected to be important in producing DNA damage and mutations, the LET is dominated by the so-called indirect events.

The average distribution of secondary electrons as a function of radial distance can be used to evaluate the contribution from indirect events using a folding approach. We treat this spectrum as an isotropic source incident on the sensitive volume. The theoretical evaluation of microdosimetric spectra from electrons is difficult to treat analytically because of the small mean free path of electrons for both elastic and inelastic collisions and the importance of energy and range straggling for electrons. Extensive measurements of event spectra using photons and in some cases electrons over a large range of energies have been made with TEPC's (refs. 20–22). For smaller site sizes, Monte-Carlo calculations have been made for electrons with energies from 0.1 to 100 keV (refs. 6 and 7). Our approach is to consider the average electron spectrum of electrons at radial distance t from the path of the ion and fold this distribution with representations of measurements for photons or electrons. In this way, local fluctuations in energy deposition from delta rays are taken into account.

The event spectrum from indirect events is found by assuming the radial distribution of electrons is incident on a spherical site at distance t from the track center and folding this spectrum with the event spectrum for electrons of a given energy

$$f_{\text{out}}(y, t) = \int dE\ \phi(t, E) f_{e^-}(E, y) \tag{16}$$

where the distributions $f_{e^-}(E, y)$ are the events by electrons of energy E in a particular volume as inferred from experiments (refs. 20–22).

The y spectra from measurements with photons are parameterized as

$$f(E, y) = N\left[c \exp\left(\frac{-y}{a}\right) + (1 - c) \exp\left(\frac{-y}{b}\right)^2\right] \tag{17}$$

with N as a normalization constant and the parameters chosen as $b = 6.5$ keV/μm, and

$$a = a_1 + a_2 \exp\left(-\frac{E_{\text{photon}}}{60}\right)^{1/2} \tag{18}$$

$$c = 1 - c_0\left[1 - \exp\left(-\frac{E_{\text{photon}}}{1000}\right)\right] \tag{19}$$

Values for the parameters a_1, a_2, and c_0 are given in table 1 for several spherical sites with diameters from 0.5–4.0 μm. Equation (17) provides a good approximation to measured values for y_F and y_D as a function of photon energy as shown in figure 6. For an exponential spectrum, the relationship $y_D/y_F = 2$ is found and is observed in most experiments below 100 keV. The photon spectrum of equation (17) is fit to experiments for photon irradiation in walled counters. Some differences in the response of walled and wallless counters for photons and electrons should be expected and are not described here. To relate the photon energy to its secondary electrons we use the

average secondary electron energy from photon irradiation resulting from Compton scattering and the photoelectric effect. Event spectrum with photons for wall-less counters indicates about a 10- to 20-percent reduction in y_F in comparison to walled counters. Also, measurements made directly with electron beams (refs. 21 and 22) suggest slightly lower values for y_F and y_D than those derived here from photon exposures. The modification of equation (18) to $a_{\text{wall-less}} \approx 0.8a_{\text{wall}}$ will approximately account for some of these differences; however, such effects need to be studied further. The total event spectrum is found by integrating overall radial distances and including the contribution from direct events.

Table 1. Parameters for Photon Lineal Energy Distribution

Site diameter, μm	a_1	a_2	c_0
0.5	0.3	4.6	0.0050
1.0	0.14	4.2	0.0015
2.0	0.14	3.4	0.0010
4.0	0.18	2.6	0.0005

Results and Discussion

Figure 7(a) shows the frequency average of the specific energy, $z_F(t)$ as a function of radial distance from the path of 600 MeV/amu iron ion for a site of 1.3 μm diameter. The lineal energy spectrum described above is converted to specific energy using the relationship

$$z = 0.204 \frac{y}{d^2} \tag{20}$$

where z is in Gy, y is in keV/μm, and d is the site diameter in μm. Good agreement with the experiment of Metting et al. (ref. 23) is found. The frequency-averaged values and their correlation with known values for electrons and photons clearly indicate the role of delta rays in outside events. Figure 7(b) shows comparisons of calculation to experiment for the mean square of the specific energy, which is given by

$$z_D^2(t) = z_D(t)\, D(t) + D^2(t) \tag{21}$$

Again good agreement between experiment and model is found. Figure 8 shows comparisons of model to experiments (ref. 24) for $z_D(t)$ for 13.7 MeV/amu germanium ions in 0.5 and 1.0 μm sites. Comparison of figures 7 and 8 indicates a harder electron spectrum for lower energy ions. The comparisons of the radial distribution for average specific energy provide new support for the success of the average-track model of Katz (refs. 5 and 9) in describing relative biological effectiveness for diverse radiation fields. These comparisons indicate that models that describe local fluctuations in energy deposition would account for factors responsible for the small differences in response seen between gamma-rays and hard X rays. For a parametric model summing the effects of expansive electron spectra such differences may be of reduced importance; however, such differences could be described in the present approach.

Figures 9–11 show calculations of the frequency- and dose-averaged linear energy versus kinetic energy for proton, oxygen, and iron beams. Also shown are values of the LET. High-energy proton beams are seen to have much higher values for y_F and y_D than LET, with y_D exceeding LET by a factor of about 5 at high energies in a 1 μm site. Such difference will have large impact in validating radiation transport codes (refs. 25 and 26) with TEPC measurement (ref. 2). For heavy ions, values of y_D agree with LET within 20 percent; however, these ions carry an additional low y component to their spectrum as shown in figure 12. Such observations were seen in the experiments of Dicello, Wasiolek, and Zaider (ref. 27) and the present model provides an analytic model to describe these effects. For studying energy deposition from relativistic ions, the use of large site sizes (>1 μm) would not significantly diminish the contribution of indirect events. For space radiation studies, large site sizes would further distort contributions from low velocity ions produced through target fragmentation (ref. 26).

Conclusions

The average-track model has been extended to describe the radial distribution of electrons about the path of an ion. We have used this spectrum in a folding model to predict the contribution of indirect events to frequency-event spectra. In this method, local fluctuations in energy deposition are included in the model. Tissue equivalent proportional counters are often used to measure the spectrum of radiation types onboard spacecraft or in the upper atmosphere. The method used here will provide response functions to validate the results of radiation transport codes and

environmental models with such measurements. Large differences between linear energy and lineal energy spectra for relativistic ions are expected, based on the model described, because of indirect events. Most importantly, high-energy light ions have significantly increased values for frequency- and dose-averaged lineal energies compared to LET. Finally, we have discussed differences in track width, secondary electron spectrum, and frequency event spectrum for ions of identical LET. Clearly these differences, along with other noted track structure effects, preclude the use of LET or Z^{*2}/β^2 as descriptors of radiation quality.

NASA Langley Research Center
Hampton, VA 23681-2199
April 6, 1998

Reference

1. Cucinotta, F. A.; Wilson, J. W.; Katz, R.; Atwell, W.; Badhwar, G. D.; and Shavers, M. R.: Track Structure and Radiation Transport Model for Space Radiobiology Studies. *Adv. Space Res.*, vol. 18, no. 12, 1996, pp. 183–194.

2. Badhwar, G. D.; Cucinotta, F. A.; Braby, L. A.; and Konradi, A.: Measurements on the Shuttle of the LET Spectra of Galactic Cosmic Radiation and Comparison With the Radiation Transport Model. *Radiat. Res.*, vol. 139, no. 3, 1994, pp. 344–351.

3. Hamm, R. N.; Turner, J. E.; Wright, H. A.; and Ritchie, R. H.: Heavy-Ion Track Structure in Silicon. *IEEE Trans. Nucl. Sci.*, vol. NS-26, no. 6, Dec. 1979, pp. 4892–4895.

4. Kobetich, E. J.; and Katz, Robert: Energy Deposition by Electron Beams and δ Rays. *Phys. Rev.*, vol. 170, no. 2, June 1968, pp. 391–396.

5. Katz, R.; Ackerson, B.; Homayoonfar, M.; and Sharma, S. C.: Inactivation of Cells by Heavy Ion Bombardment. *Radiat. Res.*, vol. 47, 1971, pp. 402–425.

6. Cucinotta, F. A.; Wilson, J. W.; Shavers, M. R.; and Katz, R.: Effects of Track Structure and Cell Inactivation on the Calculation of Heavy Ion Mutation Rates in Mammalian Cells. *Internat. J. Radiat. Biol.*, vol. 69, no. 5, May 1996, pp. 593–600.

7. Goodhead, D. T.: Initial Events in the Cellular Effects of Ionizing Radiations: Clustered Damage in DNA. *Internat. J. Radiat. Biol.*, vol. 65, no. 1, Jan. 1994, pp. 7–18.

8. Nikjoo, H.; O'Neill, P. O.; Goodhead, D. T.; and Terissol, M.: Computational Modelling of Low Energy Electron Induced DNA Damage by Early Physical and Chemical Events. *Int. J. Radiat.*, vol. 71, 1997, pp. 467–483.

9. Katz, R.: RBE, LET, and Z/β^{α}. *Health Phys.*, vol. 18, no. 2, 1970, p. 170.

10. Schäfer, M.; Schmitz, C.; and Bücker, H.: DNA Double Strand Breaks Induced in Escherichia Coli Cells by Radiations of Different Quality. *Radiat. Prot. Dosim.*, vol. 52, nos. 1–4, 1994, pp. 233–236.

11. Kiefer, J.; Stoll, U.; and Schneider E.: Mutation Induction by Heavy Ions. *Adv. Space Res.*, vol. 14, no. 10, Oct. 1994, pp. 257–266.

12. Belli, M.; Moschini, G.; Tabocchini, M. A.; Simone, G.; Sapora, O.; Tiverson, P.; Ianzini, F.; Haque, A. M. I.; Cherubini, R.; and Cera, F.: Inactivation and Mutation Induction in V79 Cells by Low Energy Protons: Re-Evaluation of the Results at the LNL Facility. *Internat. J. Radiat. Biol.*, vol. 63, no. 3, Mar. 1993, pp. 331–338.

13. Brenner, D. J.; Zaider, M.; Dicello, J. F.; and Bichsel, H.: Theoretical Approaches to Energy Deposition in Small Sites. *Seventh Symposium on Microdosimetry*, J. Booz, H. E. Ebert, and H. D. Hartfiel, eds., LALS, 1981, pp. 677–688.

14. Wilson, W. E.; Metting, N. F.; and Paretzke, H. G.: Microdosimetric Aspects of 0.3- to 10-MeV Proton Tracks. *Radiat. Res.*, vol. 115, 1988, pp. 389–402.

15. Wilson, J. W.; Cucinotta, F. A.; and Hajnal, F.: Analytic Relationships of Nuclear Field Microdosimetric Quantities for Target Fragmentation in Tissue Systems. *Health Phys.*, vol. 60, no. 4, 1991, pp. 559–565.

16. Cucinotta, Francis A.; Katz, Robert; Wilson, John W.; and Dubey, Rajendra R.: *Heavy Ion Track-Structure Calculations for Radial Dose in Arbitrary Materials.* NASA TP-3497, 1995.

17. Cheung, Wang K.; and Norbury, John W.: *Stopping Powers and Cross Sections Due to Two-Photon Processes in Relativistic Nucleus-Nucleus Collisions.* NASA CR-4574, 1994.

18. Brandt, Werner; and Ritchie, R. H.: Primary Processes in the Physical Stage. *Physical Mechanisms in Radiation Biology*, U.S. Atomic Energy Comm., 1974, pp. 20–46.

19. Goodhead, D. T.; and Nikjoo, H.: Current Status of Ultrasoft X-Rays and Track Structure Analysis as Tools for Testing and Developing Biophysical Models of Radiation Action. *Radiat. Prot. Dosim.*, vol. 31, nos. 1–4, May 1989, pp. 343–350.

20. Booz, J.; Ebert, H. G.; and Smith, B. G. R., eds.: Microdosimetric Spectra and Parameters of Low LET-Radiations. *Fifth Symposium on Microdosimetry*, EUR-5452, Vol. 1, Comm. European Comm., 1976, pp. 311–345.

21. Haque, A. K. M.; and Saqan, S. A.: Microdosimetric Study With Cylindrical Walled and Wall-less Proportional Counters. *Sixth Symposium on Microdosimetry*, J. Booz and H. G. Ebert, eds., Comm. European Comm., May 1978.

22. Braby, L. A.; and Roesch, W. C.: Direct Measurement of f(z) for Fast Electrons. *Sixth Symposium on Microdosimetry*, J. Booz and H. G. Ebert, eds., Comm. European Comm., May 1978.

23. Metting, N. F.; Rossi, H. H.; Braby, L. A.; Kliauga, P. J.; Howard, J.; Zaider, M.; Schimmerling, W.; Wong, M.; and Rapkin, M.: Microdosimetry Near the Trajectory of High-Energy Heavy Ions. *Radiat. Res.*, vol. 116, 1988, pp. 183–195.

24. Metting, Noelle Frances: Studies of Radiation-Induced Mutagenesis and Cell Cycle Perturbation. Ph.D. Thesis, Harvard Univ., 1994.

25. Wilson, John W.; Townsend, Lawrence W.; Schimmerling, Walter; Khandelwal, Govind S.; Khan, Ferdous; Nealy, John E.; Cucinotta, Francis A.; Simonsen, Lisa C.; Shinn, Judy L.; and Norbury, John W.: *Transport Methods and Interactions for Space Radiations*. NASA RP-1257, 1991.

26. Cucinotta, F. A.; Wilson, J. W.; Shinn, J. L.; Badavi, F. F.; and Badhwar, G. D.: Effects of Target Fragmentation on Evaluation of LET Spectra From Space Radiations: Implications for Space Radiation Protection Studies. *Radiat. Meas.*, vol. 26, no. 6, Nov. 1996, pp. 923–934.

27. Dicello, J. F.; Wasiolek, M.; and Zaider, M.: Measured Microdosimetric Spectra of Energetic Ion Beams of Fe, Ar, Ne, and C: Limitations of LET Distributions and Quality Factors in Space Research and Radiation Effects. *IEEE Trans. Nucl. Sci.*, vol. 38, no. 6, Dec. 1991, pp. 1203–1209.

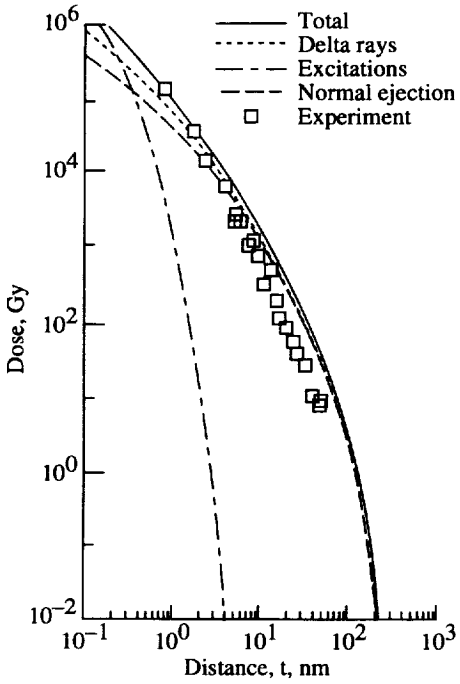

(a) For 1 MeV protons.

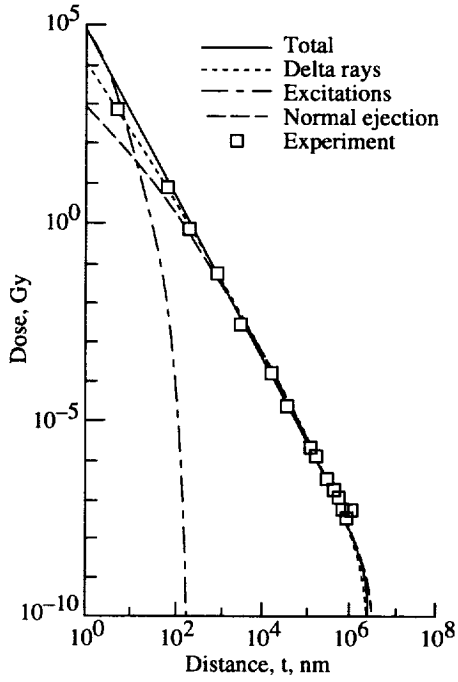

(b) For 377 MeV/amu neon.

Figure 1. Comparison of calculations to experiments for radial dose for ions of LET = 30 KeV/μm.

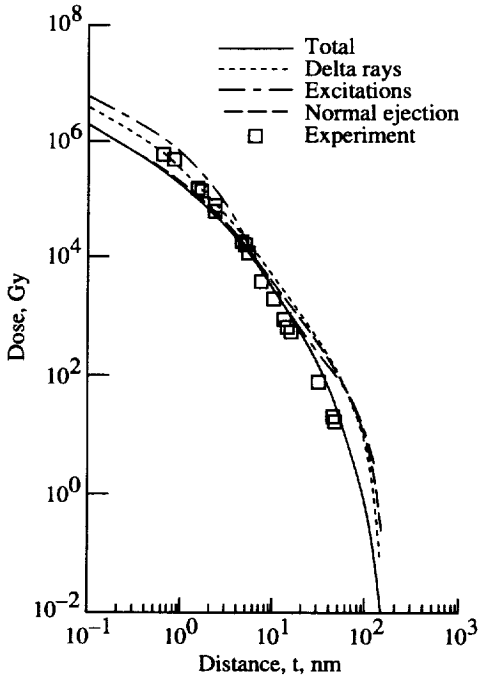

(a) For 0.75 MeV/amu alpha particles.

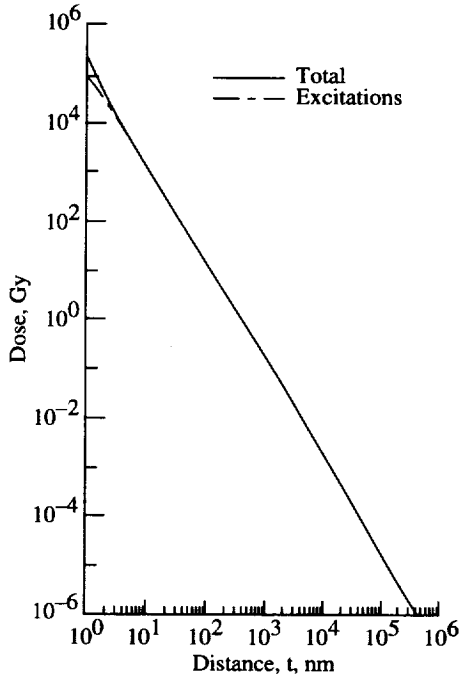

(b) For 1000 MeV/amu iron particles.

Figure 2. Calculations of radial dose distributions from ions of LET of 150 KeV/μm.

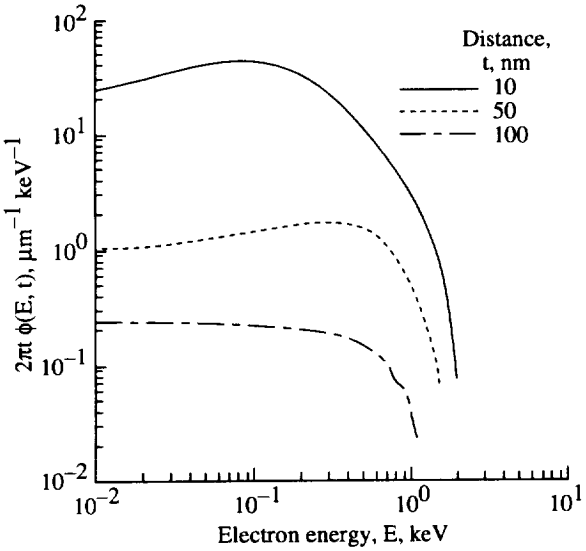

(a) Electron spectra for 1 MeV protons.

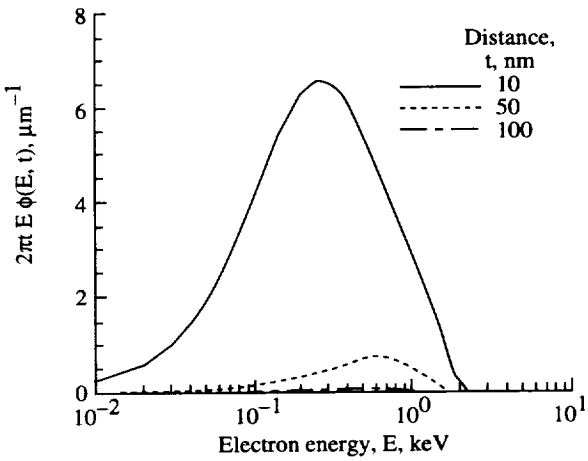

(b) Electron lethargy spectra for 1 MeV protons.

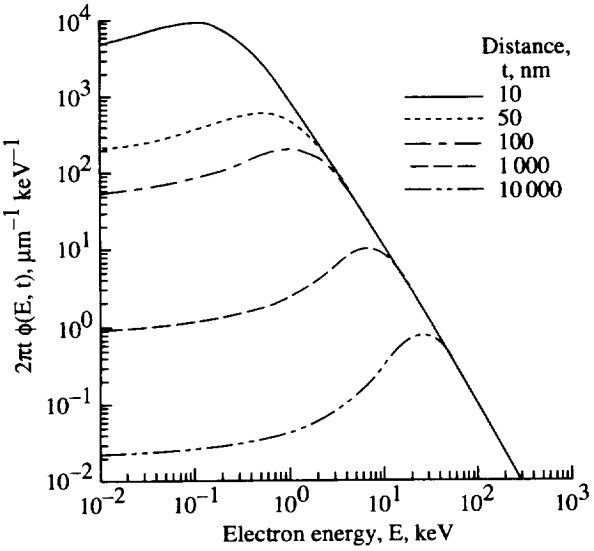

(c) Electron spectra for 377 MeV/amu neon.

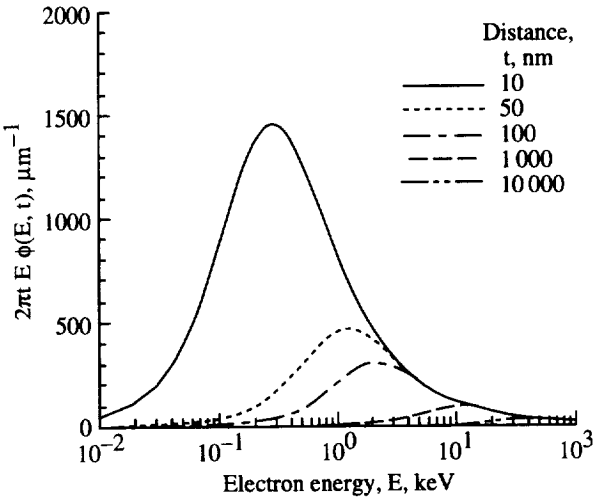

(d) Electron lethayrgy spectra for 377 MeV neon.

Figure 3. Calculations of electron energy (E) spectrum $\varphi(E, t)$ or $2\pi t\ \varphi(E, t)$ at various distances t from ions of LET of 30 keV/μm.

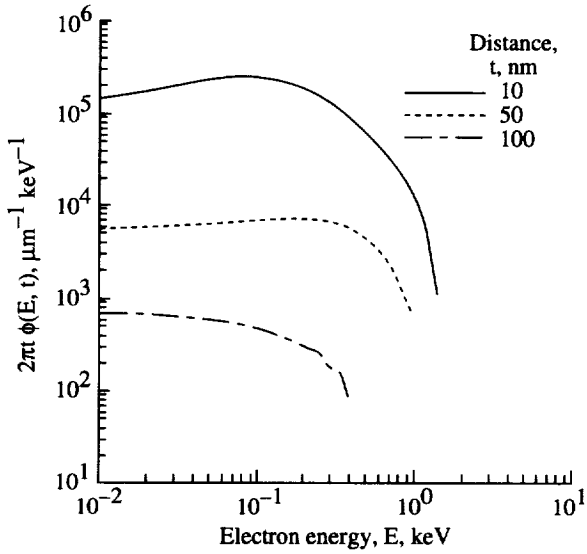

(a) Electron spectra for 0.75 MeV/amu alpha particle.

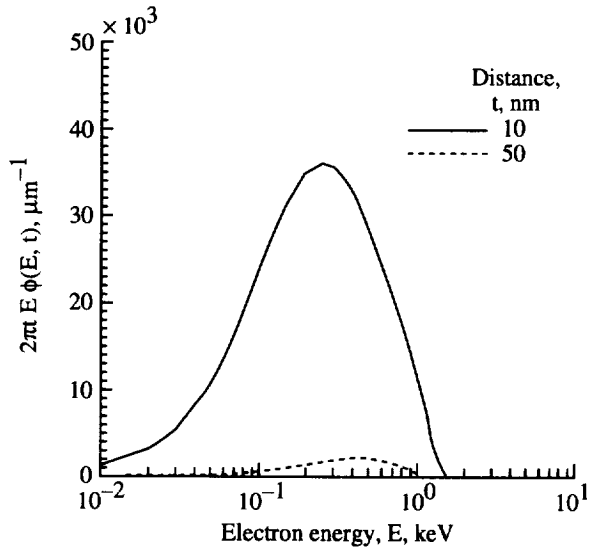

(b) Electron lethargy spectra for 0.75 MeV alpha particle.

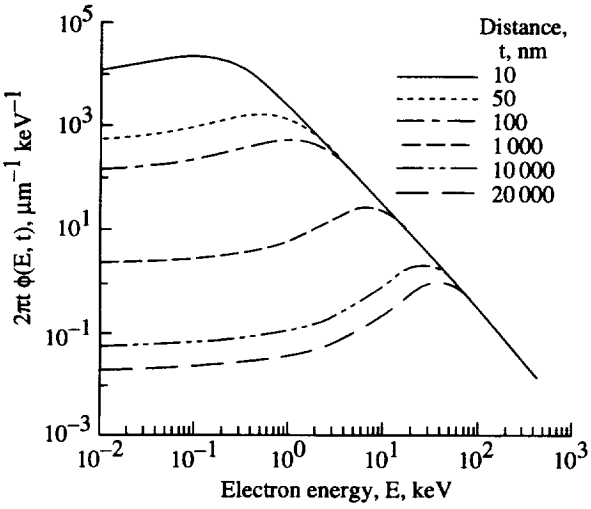

(c) Electron spectra for 1000 MeV/amu iron ions.

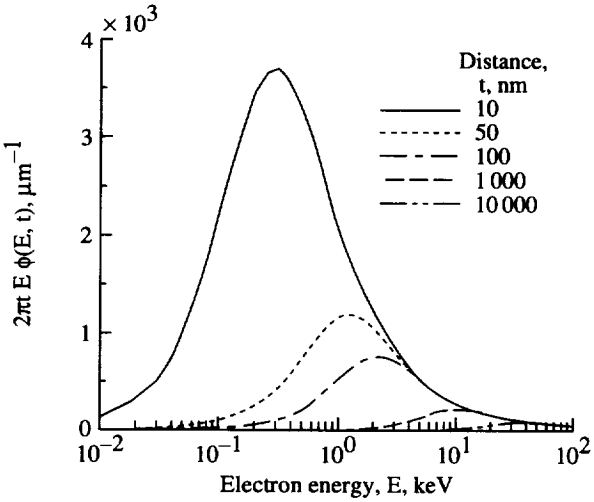

(d) Electron lethargy spectra for 1000 MeV/amu iron ions.

Figure 4. Calculations of electron energy (E) spectrum $\varphi(E, t)$ or $2\pi t\ \varphi(E, t)$ at various distances t from ions of LET of 150 keV/μm.

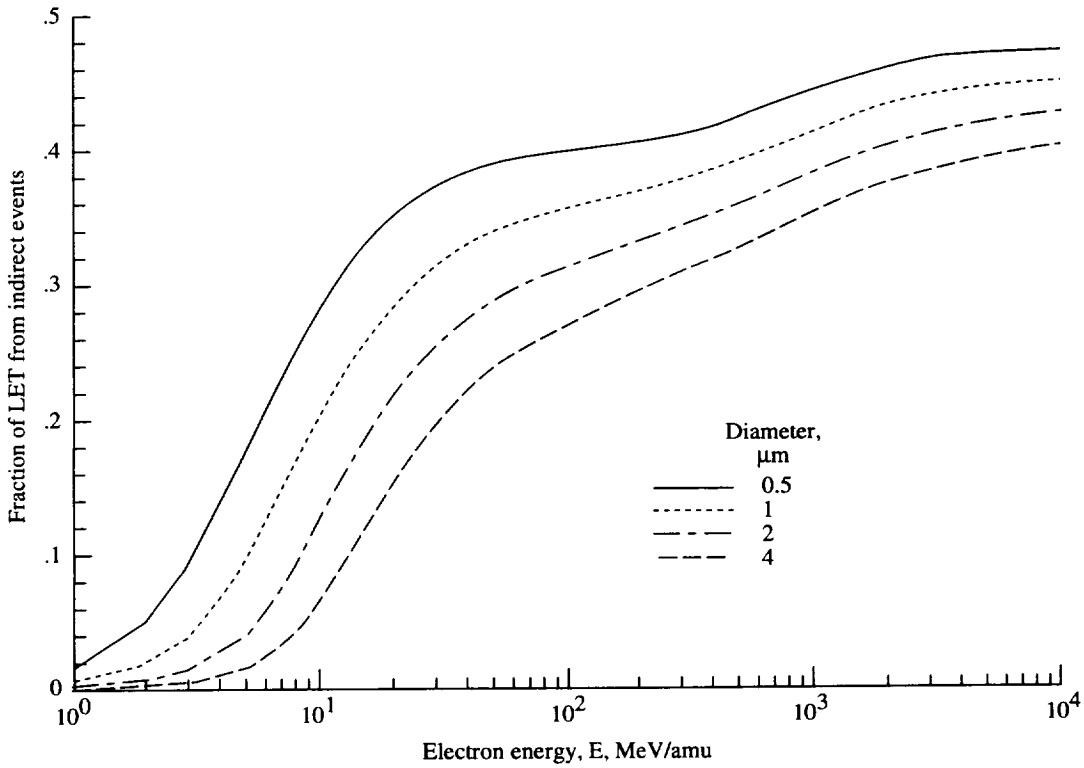

Figure 5. Calculation of fraction of LET versus kinetic energy from indirect events for iron ions in spherical sites of various diameters.

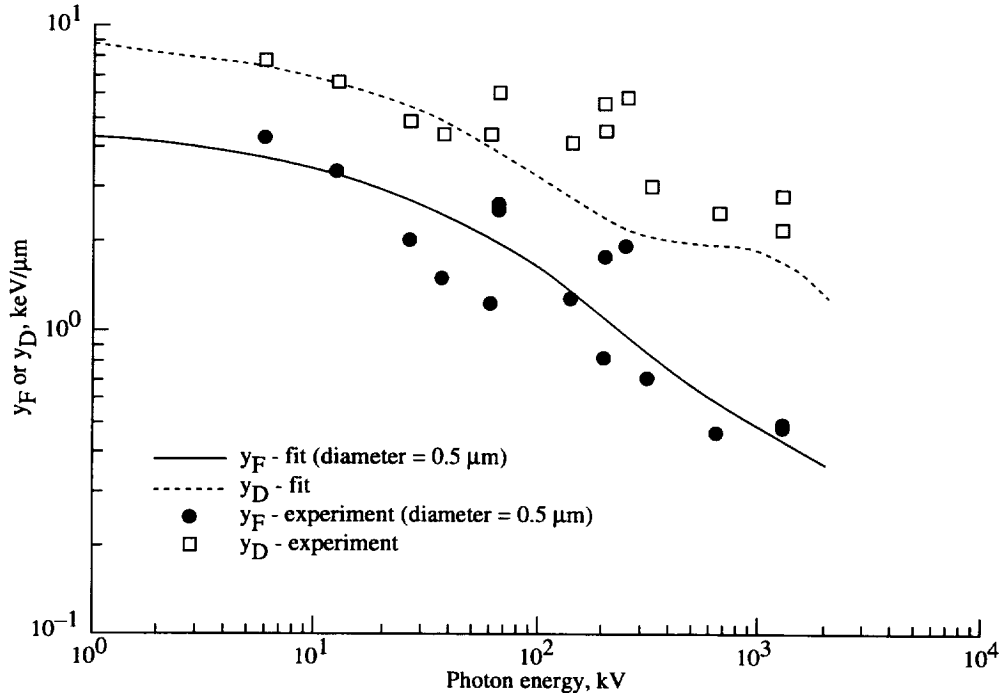

(a) Diameter = 0.5 μm.

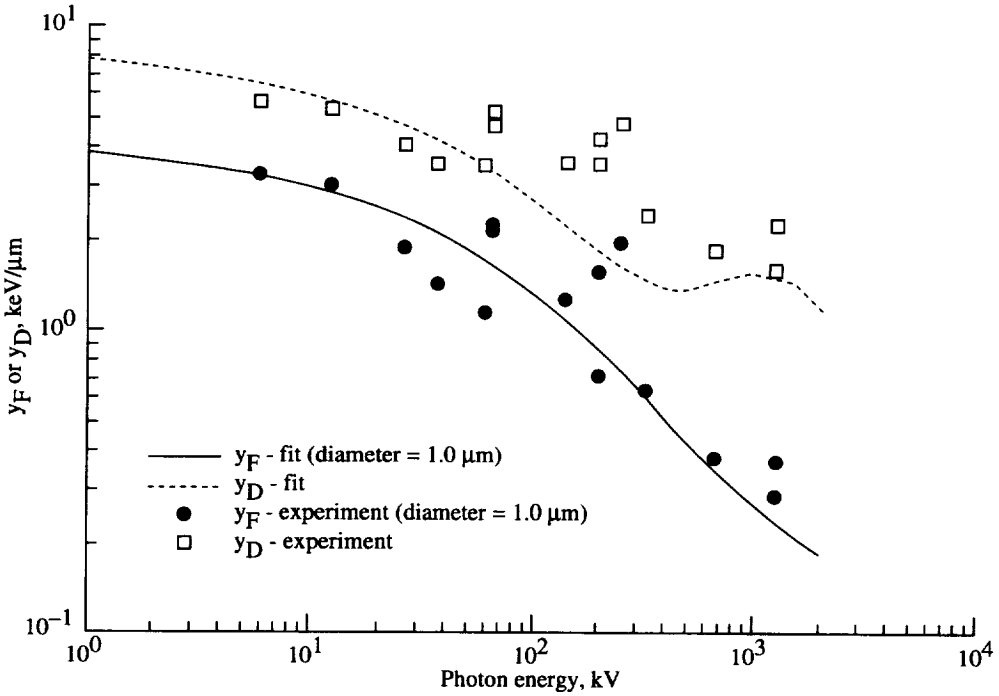

(b) Diameter = 1 μm.

Figure 6. Comparison of parametric model to experiments for frequency-averaged lineal energy (y_F) and dose-averaged lineal energy (y_D) versus photon energy.

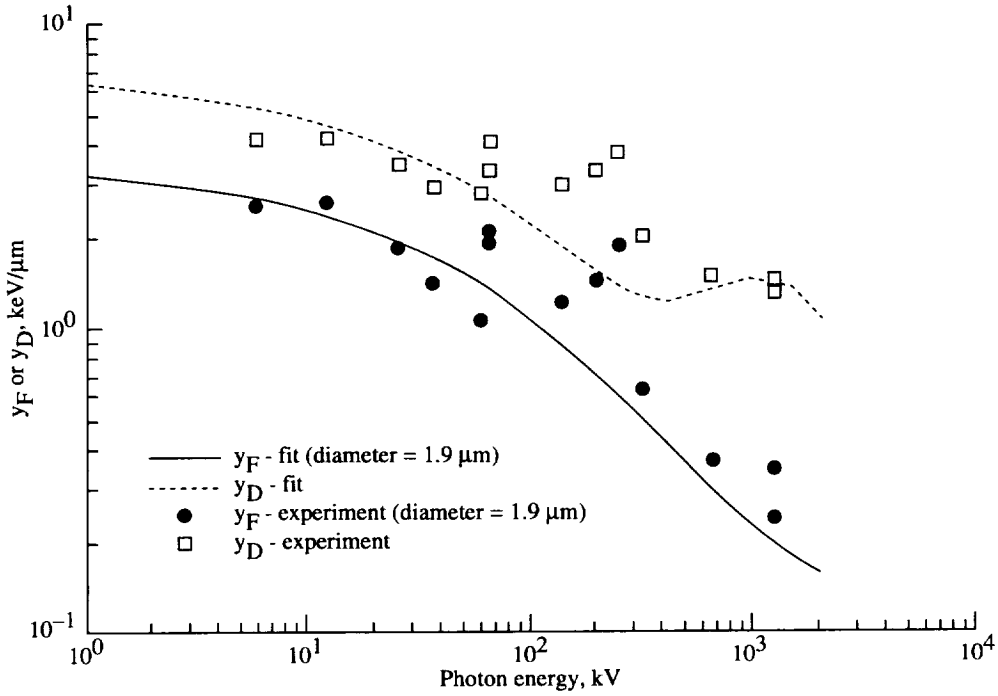

(c) Diameter = 2 μm.

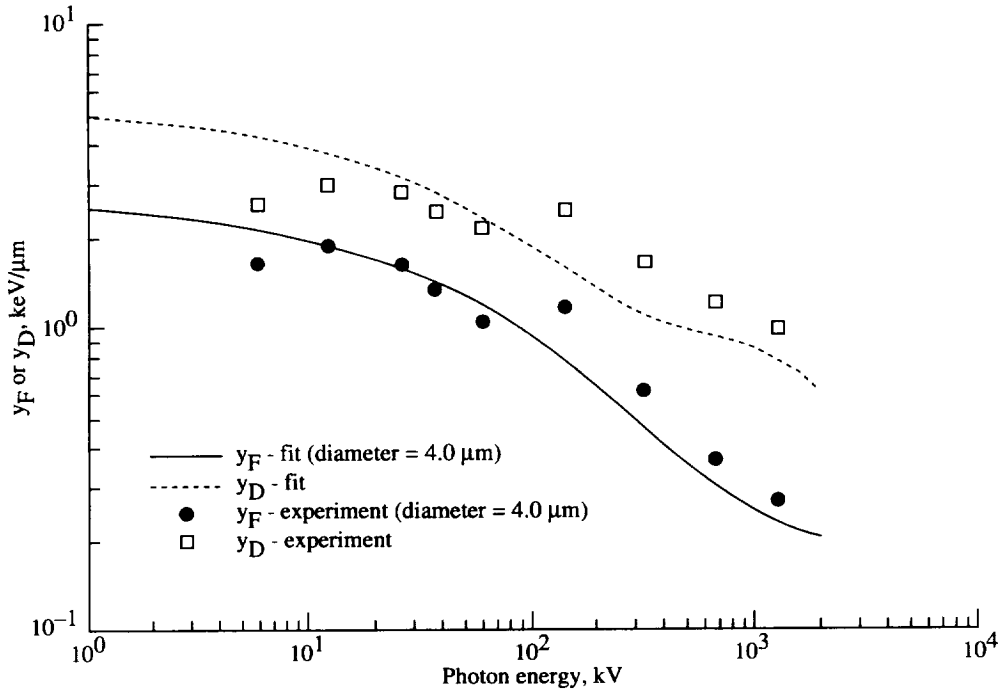

(d) Diameter = 4 μm.

Figure 6. Concluded.

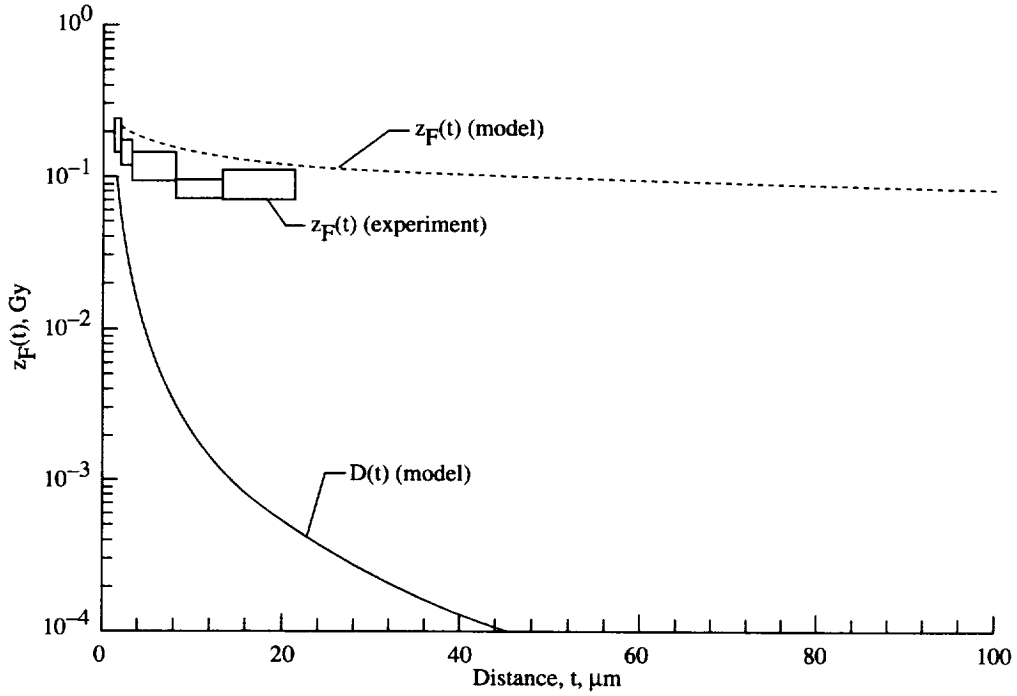

(a) Average specific energy, $z_F(t)$.

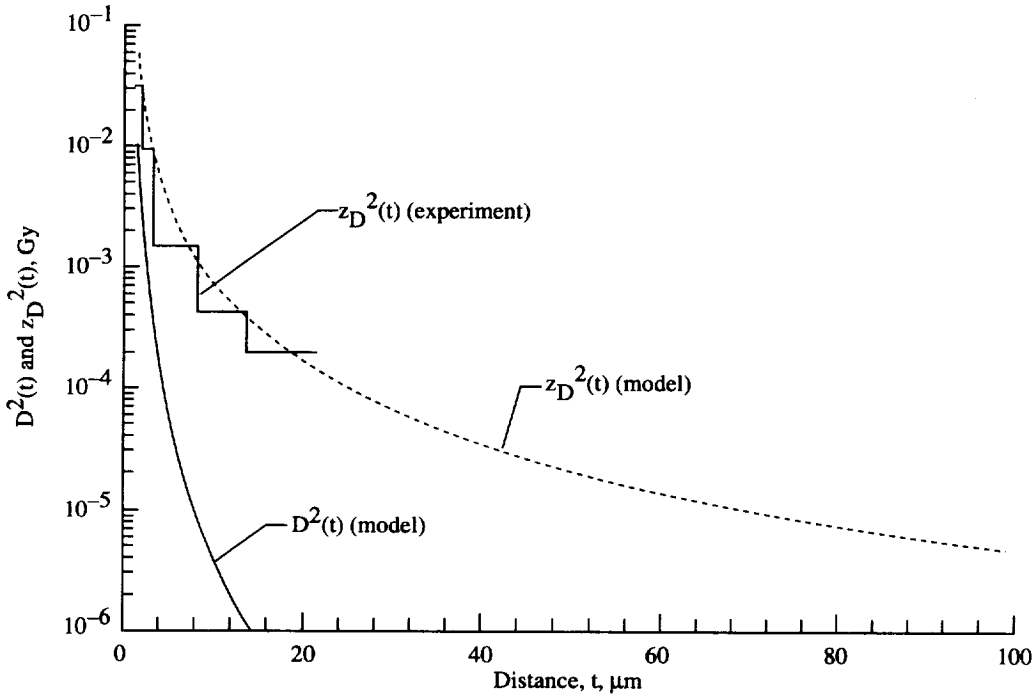

(b) Square of mean specific energy.

Figure 7. Comparison of calculation to experiments (ref. 23) for average energy in 1.3 μm site as function of radial distance t for 600 MeV/amu iron ions.

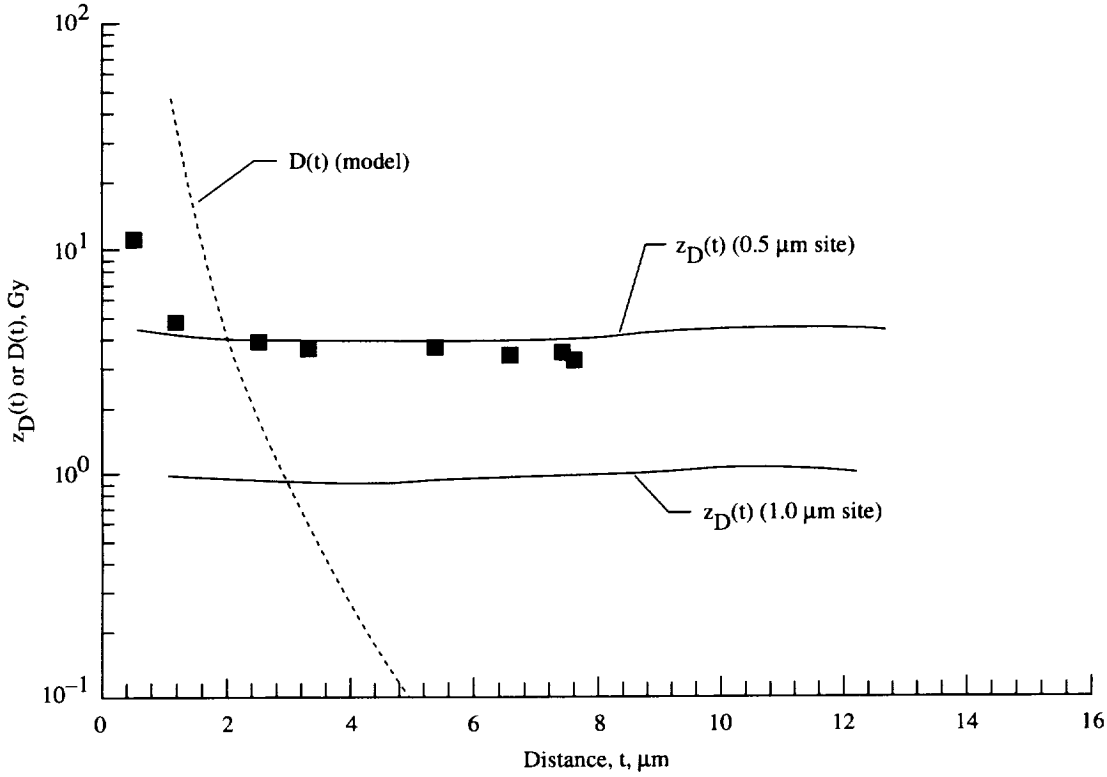

Figure 8. Comparison of calculation to experiment (ref. 24) for average specific energy in 0.5 and 1.0 μm sites as function of radial distance for 13.7 MeV/amu germanium ions.

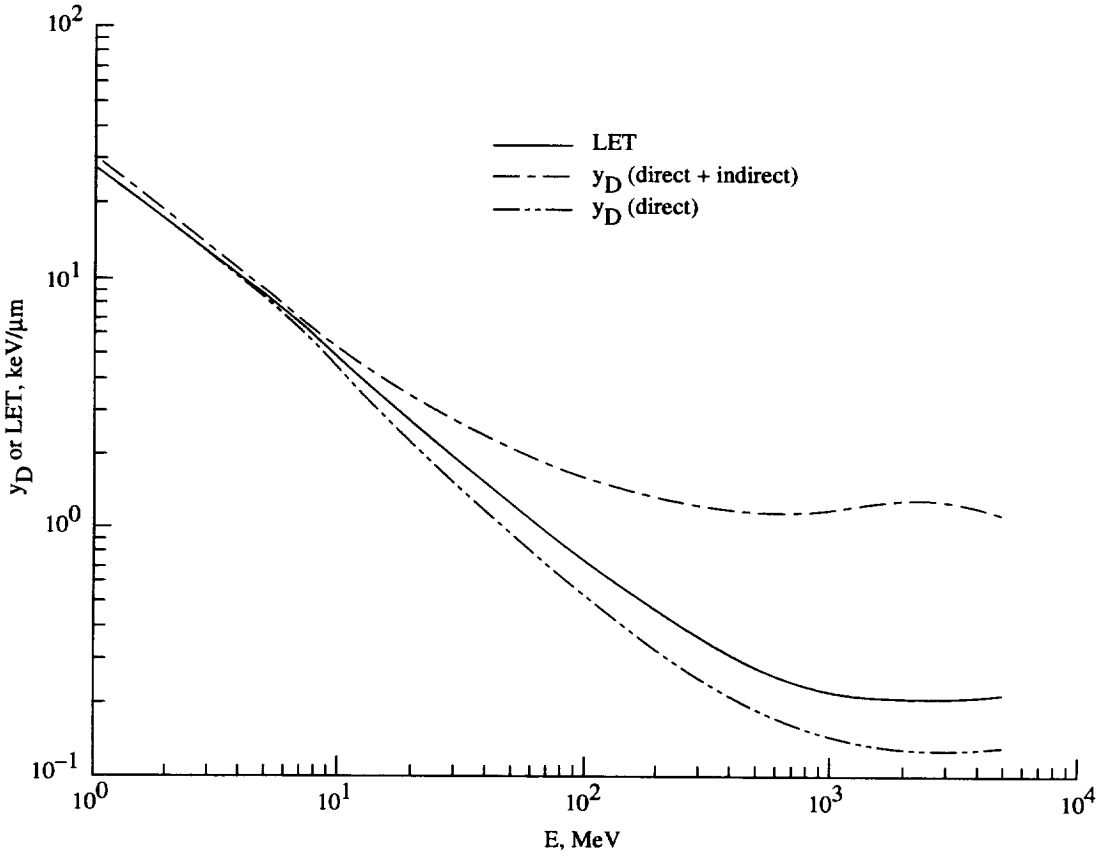

(a) Diameter = 1 μm.

Figure 9. Calculations of dose-averaged lineal energy (y_D) versus kinetic energy for protons in spherical sites.

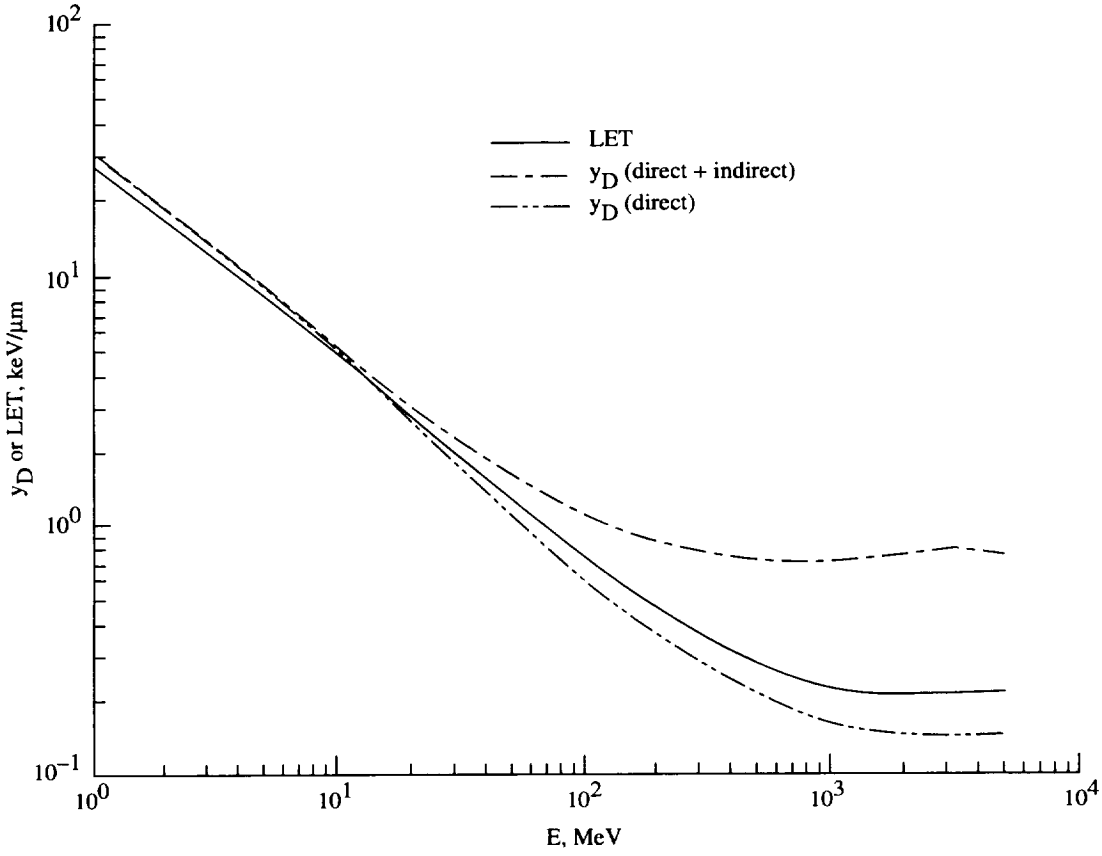

(b) Diameter = 4 μm.

Figure 9. Concluded.

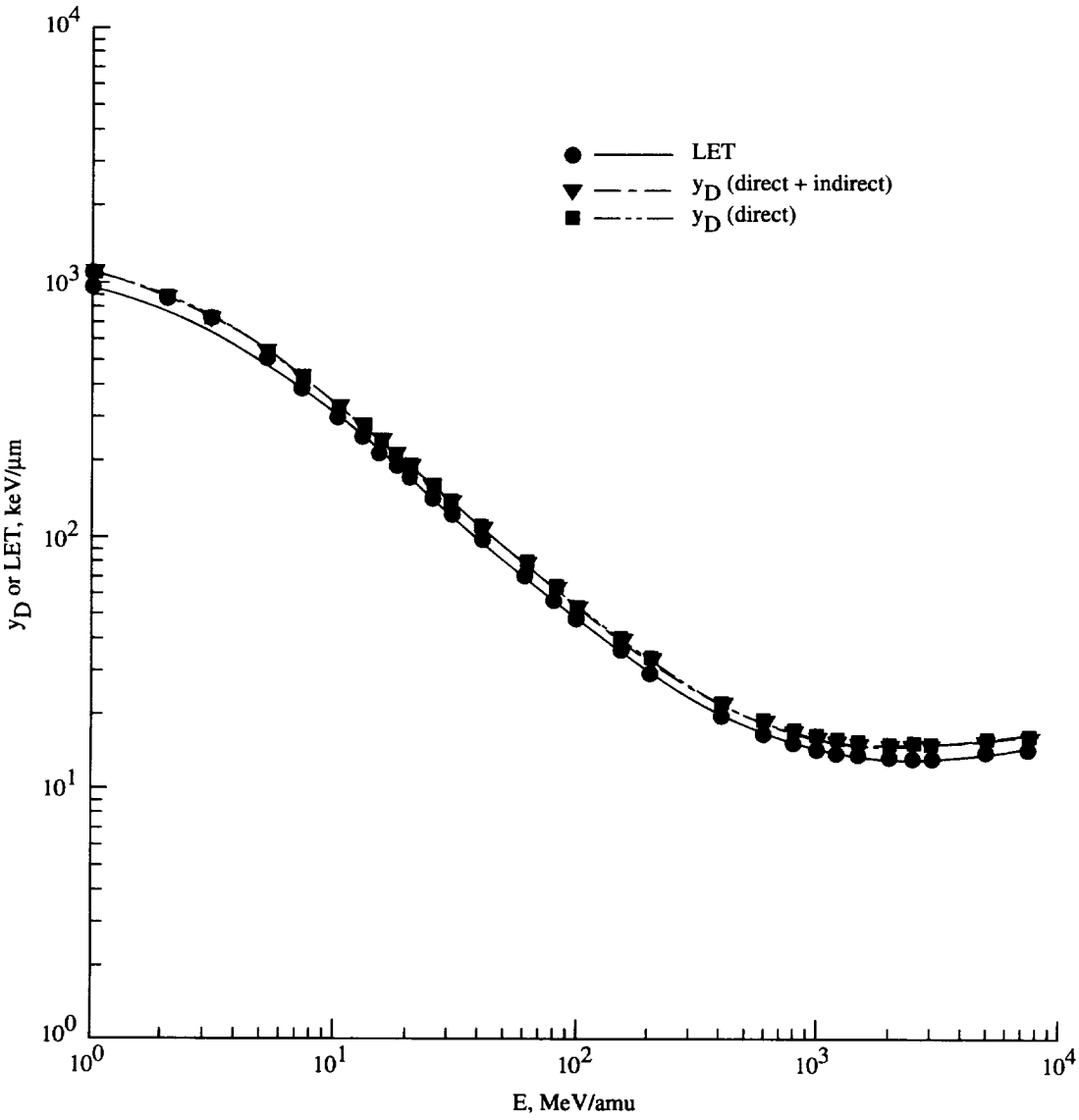

Figure 10. Calculations of dose-averaged lineal energy (y_D) versus kinetic energy for oxygen ions in 1 μm sites.

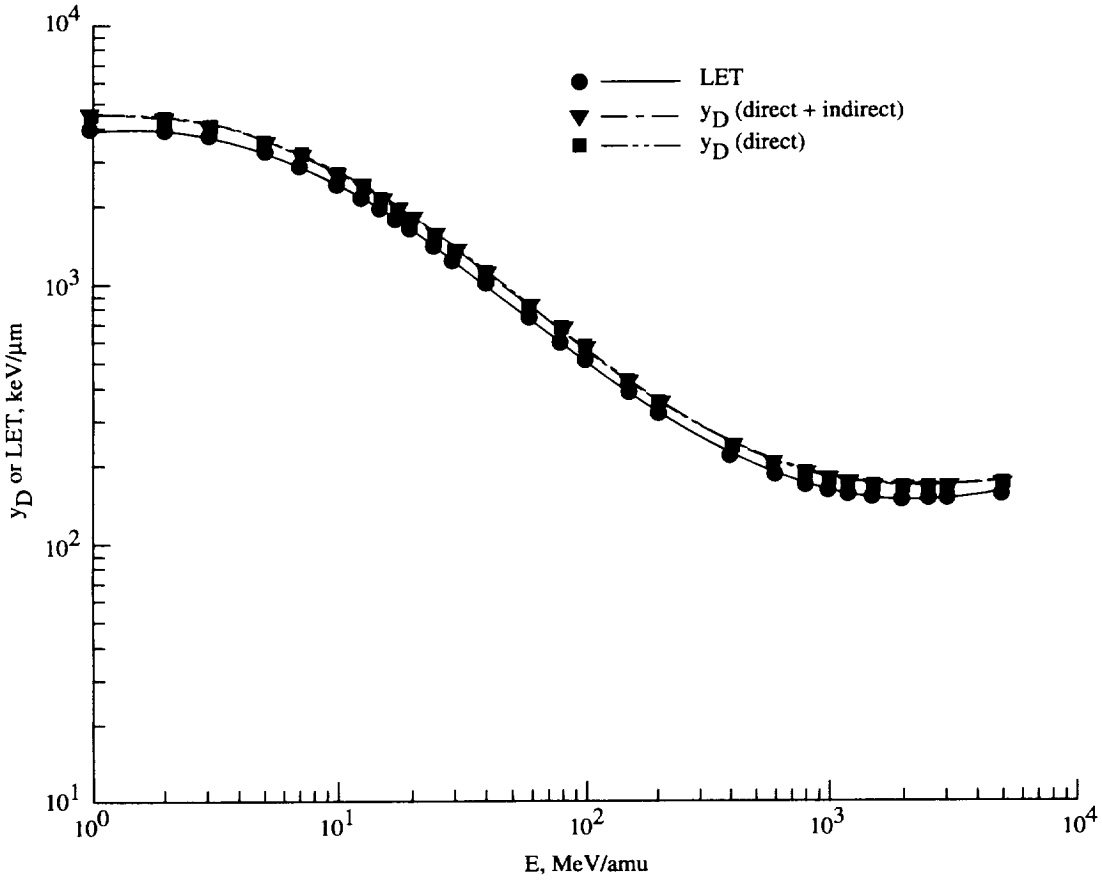

Figure 11. Calculations of dose-averaged lineal energy (y_D) versus kinetic energy for iron ions in 1 μm sites.

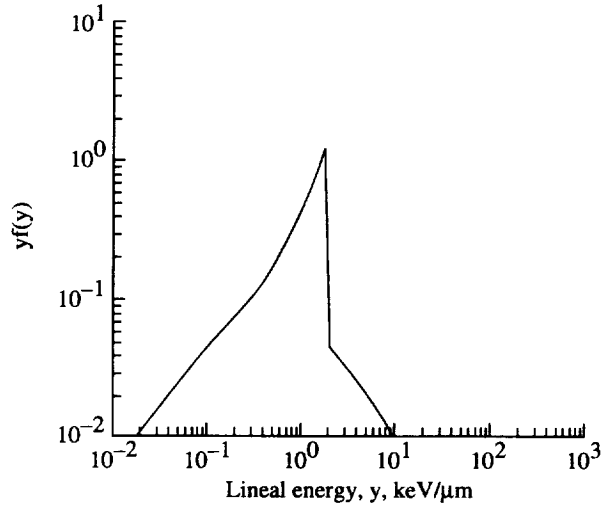

(a) Helium.

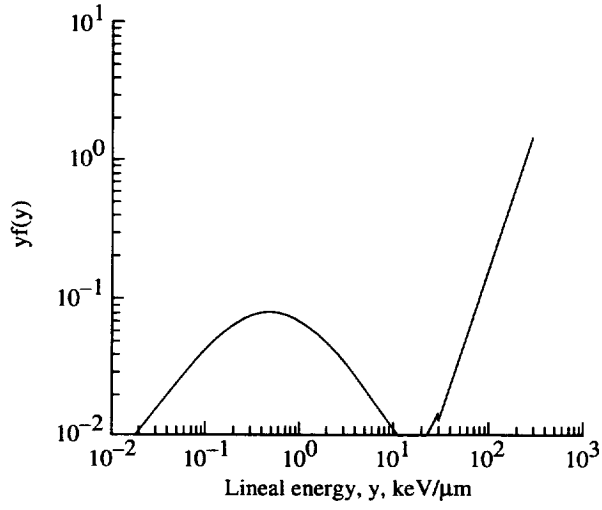

(b) Iron.

Figure 12. Comparison of event distributions, $yf(y)$, in 1 μm site for helium and iron ions of 200 MeV/amu.

REPORT DOCUMENTATION PAGE

Form Approved
OMB No. 07704-0188

1. AGENCY USE ONLY *(Leave blank)*	2. REPORT DATE	3. REPORT TYPE AND DATES COVERED
	September 1998	Technical Publication

4. TITLE AND SUBTITLE
Track Structure Model for Radial Distributions of Electron Spectra and Event Spectra From High-Energy Ions

5. FUNDING NUMBERS
WU 199-45-16-11

6. AUTHOR(S)
F. A. Cucinotta, R. Katz, and J. W. Wilson

7. PERFORMING ORGANIZATION NAME(S) AND ADDRESS(ES)
NASA Langley Research Center
Hampton, VA 23681-2199

8. PERFORMING ORGANIZATION REPORT NUMBER
L-17655

9. SPONSORING/MONITORING AGENCY NAME(S) AND ADDRESS(ES)
National Aeronautics and Space Administration
Washington, DC 20546-0001

10. SPONSORING/MONITORING AGENCY REPORT NUMBER
NASA/TP-1998-208707

11. SUPPLEMENTARY NOTES
Cucinotta and Wilson: NASA Langley Research Center, Hampton, VA; Katz: University of Nebraska, Lincoln, NE.

12a. DISTRIBUTION/AVAILABILITY STATEMENT
Unclassified–Unlimited
Subject Category 93 Distribution: Standard
Availability: NASA CASI (301) 621-0390

12b. DISTRIBUTION CODE

13. ABSTRACT ***(Maximum 200 words)***

An analytic method is described for evaluating the average radial electron spectrum and the radial and total frequency-event spectrum for high-energy ions. For high-energy ions, indirect events make important contributions to frequency-event spectra. The method used for evaluating indirect events is to fold the radial electron spectrum with measured frequency-event spectrum for photons or electrons. The contribution from direct events is treated using a spatially restricted linear energy transfer (LET). We find that high-energy heavy ions have a significantly reduced frequency-averaged lineal energy (y_F) compared to LET, while relativistic protons have a significantly increased y_F and dose-averaged lineal energy (y_D) for typical site sizes used in tissue equivalent proportional counters. Such differences represent important factors in evaluating event spectra with laboratory beams, in space-flight, or in atmospheric radiation studies and in validation of radiation transport codes. The inadequacy of LET as descriptor because of deviations in values of physical quantities, such as track width, secondary electron spectrum, and y_D for ions of identical LET is also discussed.

14. SUBJECT TERMS
Space radiation; Microdosimentry; High-energy ions; Radiation transport codes

15. NUMBER OF PAGES
25

16. PRICE CODE
A03

17. SECURITY CLASSIFICATION OF REPORT	18. SECURITY CLASSIFICATION OF THIS PAGE	19. SECURITY CLASSIFICATION OF ABSTRACT	20. LIMITATION OF ABSTRACT
Unclassified	Unclassified	Unclassified	

NSN 7540-01-280-5500

Standard Form 298 (Rev. 2-89)
Prescribed by ANSI Std. Z39-18
298-102